PHYSICAL REVIEW E **84**, 031108 (2011)

Noise associated with nonconservative forces in optical traps

Michel de Messieres, Natalia A. Denesyuk, and Arthur La Porta*
Department of Physics, Institute for Physical Science and Technology Biophysics Program, University of Maryland, College Park, Maryland 20742, USA

(Received 10 December 2009; revised manuscript received 29 July 2011; published 6 September 2011)

It is known that for a particle held in an optical trap the interaction of thermal fluctuations with a nonconservative scattering force can cause a persistent nonequilibrium probability flux in the particle position. We investigate position fluctuations associated with this nonequilibrium flux analytically and through simulation. We introduce a model which reproduces the nonequilibrium effects, and in which the magnitude of additional position fluctuations can be calculated in closed form. The ratio of additional nonconservative fluctuations to direct thermal fluctuations scales inversely with the square root of trap power, and is small for typical experimental parameters. In a simulated biophysical experiment the nonconservative scattering force does not significantly increase the observed fluctuations in the length of a double-stranded DNA tether.

DOI: 10.1103/PhysRevE.84.031108 PACS number(s): 05.40.Jc, 82.70.Dd, 87.80.Cc

I. INTRODUCTION

In a single-beam optical trap [1], a dielectric particle is confined to the focal volume by a force $\vec{F}_g$ proportional to the optical intensity gradient. The force exerted on the particle and the resulting displacement can be measured by detecting the deflection of the trapping beam [2–4]. Using this technique, the movement of a biological macromolecule attached to a trapped particle can be measured with near-angstrom precision [5]. However, the trapped particle is also subject to a scattering force $\vec{F}_s$, first noted by Ashkin [6], which cannot be expressed as the gradient of any function. Assuming the geometrical center of the trapping beam is defined as the origin of coordinates, with beam propagation in the positive z direction, the scattering force acts mainly in the $+z$ direction and causes the effective trap center to lie at positive z, typically within a wavelength of the geometrical trap center. In the limit of a small particle, the scattering force is proportional to the local intensity and decreases with distance from the beam axis. For particles that are large compared with the wavelength, the scattering force can be estimated using ray tracing, and increases with small displacement from a diffraction-limited trap center [6] (although it must ultimately decrease for large displacements). For small displacements both curves, illustrated in Fig. 1(a), have a roughly quadratic dependence on distance from the beam axis.

The scattering force acting on a small particle is maximum when the particle is on the beam axis. As a result the particle tends to fall towards negative z when a thermal fluctuation pushes it away from the beam axis, and climb towards positive z as it returns to the beam axis. This gives rise to a persistent mean circulation, a nonequilibrium flux that has been characterized as a fountain of probability, or a Brownian vortex [7,8]. (In the large-particle limit a circulation with the opposite sense of rotation is expected.) Such a nonequilibrium flux, which would not arise in a conservative system, results from the interaction of the nonconservative force with the thermal fluctuations. Recently the nonequilibrium flux associated with the scattering force has been detected in high-resolution experiments [9]. Another experimental study concluded that additional position fluctuations associated with the scattering force were too small to measure in a particular experimental realization [10]. From a fundamental point of view it is important to know if additional position fluctuations due to the scattering force would impact different types of high-precision experiments and how such fluctuations would depend on the physical parameters of the optical trap.

In this paper we introduce a simplified model of the system which allows us to identify an additional source of force fluctuations associated with the nonequilibrium flux and analytically calculate the resulting position fluctuations. This provides an analytical answer to the question raised in the original study: To what extent does the nonequilibrium probability flux influence measurements in optical traps [7]?

II. SIMPLIFIED MODEL

Our goal is to define a model system which reproduces the behavior of the nonconservative system with as simple a force field as possible. We model the gradient force as a harmonic restoring force and assume that the scattering force is axial:

$$\vec{F}(\vec{r}) = -\alpha_x x\hat{x} - \alpha_y y\hat{y} - \alpha_z z\hat{z} + F_s(\rho)\hat{z}, \qquad (1)$$

where α_i is the stiffness of the harmonic force along the i axis and $F_s(\rho)$ is the magnitude of the scattering force as a function of $\rho = \sqrt{x^2 + y^2}$. We will expand the scattering force as $F_s(\rho) = S_0 + S_2\rho^2$, where the second-order term is nonconservative because it cannot be derived from a scalar potential and does net work on a particle that moves on a closed path. For the small particle, assuming a scattering term of the form $F_0 \exp(-\rho^2/2\sigma^2)$, we have $S_2 = -F_0/2\sigma^2$, where σ is the standard deviation of the scattering force profile, which depends on both the beam profile and particle radius. For the large particle, Taylor expansion of the Ashkin form around the effective trap center gives $S_2 = 0.8F_0/{r_p}^2$, where r_p is the particle radius [6]. We will show that this model reproduces the circulation effect observed in previous studies

*alaporta@umd.edu

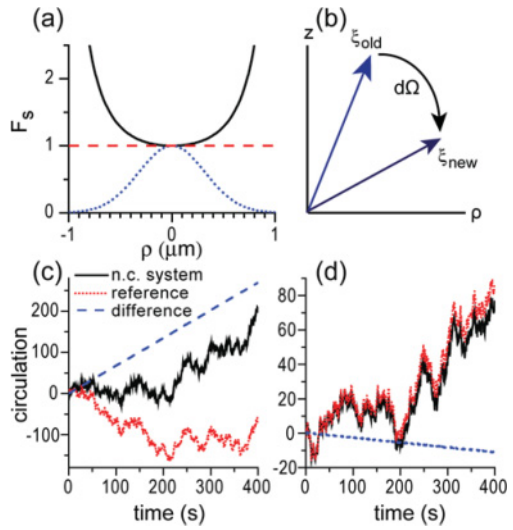

FIG. 1. (Color online). (a) Scattering force profiles for a small particle (blue dotted line) and large particle (solid black line). The small-particle curve is a Gaussian with standard deviation $\sigma = 0.32\ \mu$m and the large-particle curve is based on the ray tracing result with a particle of radius 1 μm. (b) Circulation is defined as the area swept out in the ρ-z plane, where clockwise motion is considered positive by convention. (c) Circulation obtained from the nonconservative system (solid black) and reference system (red dotted line) driven by identical thermal force fluctuations. The difference is shown in the blue dashed line. Physical parameters: $T = 298$ K, $\alpha_x = \alpha_y = 2.0$ pN/μm, $\alpha_z = 0.4$ pN/μm, time step $dt = 0.0001$ s, particle radius $r_p = 0.25\ \mu$m, and nominal scattering force given by the Gaussian function in panel (a) with $F_0 = 0.04$ pN on the beam axis. (d) Same but using the large-particle form of the scattering force with $r_p = 1.0\ \mu$m and $F_0 = 0.04$ pN on the beam axis.

while permitting important simplifications in the simulations and analytical analysis. We will also show that the analytical solution reproduces the fluctuations observed, not only in a simulation of the simplified system, but in a realistic simulation which takes into account the three-dimensional nature of the intensity gradient and scattering force fields.

The nonequilibrium probability flux in the particle position $\vec{r}$ that results from the nonconservative component of the scattering force was characterized by Roichman *et al.* in terms of the circulation Ω, as illustrated in Fig. 1(b) [7]. Each discrete measurement of $\vec{r}$ contributes a differential circulation of

$$d\vec{\Omega} = \frac{\vec{\xi}_{\text{old}} \times \vec{\xi}_{\text{new}}}{2A}, \tag{2}$$

where $\vec{\xi}$ is a two-dimensional vector defined by $\vec{\xi} = \{\rho, z\}$. The characteristic area A defines a unit of circulation, and the cross product defines the sign of circulation to be positive for clockwise motion in the ρ-z plane.

Previous work has shown that circulation is dominated by the Brownian motion of the particle, requiring very long simulation times to achieve statistical convergence [11]. However, the contribution of the nonconservative force to the circulation can be efficiently calculated by comparing results of the nonconservative system with a conservative reference system, in which the particle is subject to identical Brownian force fluctuations, but in which the nonconservative scattering force is replaced by a constant force. By looking at the difference in circulation between the original system and the reference system, circulation fluctuations arising directly from thermal forcing cancel out, isolating the circulation arising from the nonconservative force.

We use a Langevin equation of the form $\vec{F}_{\text{T}}(t) + \vec{F}(\vec{r}) - \beta\dot{\vec{r}} = 0$ to simulate the model optical trap, where β is the Stokes drag, $\vec{F}(\vec{r})$ is obtained from Eq. (1), and $\vec{F}_{\text{T}}(t)$ is a δ function-correlated stochastic noise term whose components have spectral density $|\tilde{F}_{\text{T}}(\omega)|^2 = 2k_{\text{B}}T\beta$. We define two primary nonconservative systems using the two scattering curves in Fig. 1(a) and compare them with conservative reference systems which are driven by identical thermal force fluctuations. The results are shown in Figs. 1(c) and 1(d). Thermal diffusion dominates for short times, causing large fluctuations in circulation, while the nonconservative contribution manifests itself as a linear increase in net circulation over longer times, with opposite signs for large and small particles, as expected. There is a large degree of cancellation of the circulation fluctuations when the primary and reference system are subtracted, revealing the excess circulation arising from the nonconservative term. The excess circulation obtained from subtraction of the reference system from the primary system is exactly the same as the value obtained over long time scales using a single simulation, but comparison with a matched reference system gives us additional insight into the generation of circulation, since it reveals that even over short time intervals the excess circulation accumulates at a nearly constant rate. This supports the view that the effect of the nonconservative force is a continuous biasing of fluctuations. More importantly, Figs. 1(c) and 1(d) confirm that our simplified system reproduces the nonequilibrium flux which is the essential feature of the nonconservative scattering force.

III. CALCULATION OF EXCESS FLUCTUATIONS

We now consider whether the nonconservative force results in additional fluctuations in the particle position. In the harmonic approximation, and assuming that the scattering force acts only in the positive z direction [Eq. (1)], the x-y components of the total force acting on the particle do not depend on the z coordinate. As a result, the evolution of the x-y coordinates is independent of the z motion, and is unaffected by the axial scattering force.

The independence of the transverse dynamics from the axial motion allows us to calculate the excess position fluctuations in the nonconservative system. For a simple harmonic trap, Brownian fluctuations in z are described by a thermal force F_{T} acting in a strongly damped equation of motion $F_{\text{T}}(t) - \alpha_z z - \beta\dot{z} = 0$. Using the known spectral density of the thermal force term, this gives rise to fluctuations in the z coordinate with Fourier spectral density:

$$|\tilde{z}_{\text{T}}(\omega)|^2 = \frac{|\tilde{F}_{\text{T}}(\omega)|^2}{\alpha_z^2 + \beta^2\omega^2} = \frac{2k_{\text{B}}T\beta}{\alpha_z^2 + \beta^2\omega^2}, \tag{3}$$

where similar results apply to x and y. However, in the nonconservative system the z coordinate has an additional source of noise since the scattering force depends on ρ^2 and fluctuates in time as the distance between the particle and

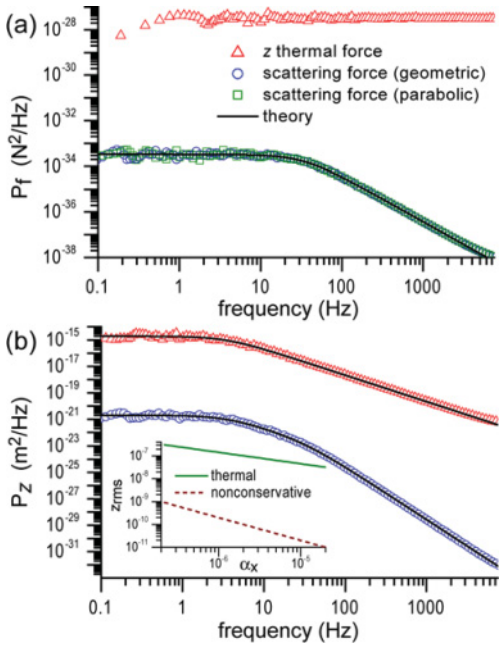

FIG. 2. (Color online). (a) Fourier spectral density of the thermal driving force (triangles) and the nonconservative z scattering force using the large-particle profile of Ashkin (circles) and its second-order Taylor expansion (squares) for dynamics obtained from numerical simulation of a Langevin equation based on Eq. (1) with the same parameters as Fig. 1. Black line: The analytical prediction for scattering force fluctuations [Eq. (4)]. (b) Fourier spectral density of the z motion driven by thermal forcing (triangles) and by the nonconservative scattering force (circles). Black lines: Analytical predictions for z fluctuations driven by thermal forcing [Eq. (3)] and the scattering force [Eq. (5)]. Inset: RMS z fluctuations arising from the thermal forcing and from the scattering force as a function of α_x, assuming α_z and F_0 are linearly related to α_x.

the beam axis varies, despite the fact that the scattering force itself has no explicit time dependence. This gives an additional fluctuating driving term for the z motion which originates entirely in the x-y dynamics of the particle. Since the x-y dynamics are independent of the z motion, this additional term, which is formally a function of ρ, is effectively a stochastic function of time, a pseudothermal forcing term which is uncorrelated with the thermal force fluctuations $F_{\mathrm{T}}(t)$ driving the z thermal motion. In contrast to $F_{\mathrm{T}}(t)$, the scattering force fluctuations manifest finite time autocorrelations determined by the continuous x-y motion, or equivalently, have a spectral density which is related to the spectral density of fluctuations in ρ^2. An extensive calculation which is detailed in the Supplemental Material [12] indicates that the nonconservative driving term arising from x fluctuations has Fourier spectral density:

$$|\tilde{F}_{\mathrm{nc}}(\omega)|^2 = \frac{8(k_{\mathrm{B}}T)^2 S_2^2}{\alpha_x \beta \left(\omega^2 + \frac{4\alpha_x^2}{\beta^2}\right)}, \tag{4}$$

where similar results are obtained for y fluctuations. The equation of z motion is linear, so the solution can be decomposed into components arising from the thermal driving term [Eq. (3)] and the nonconservative driving term. The spectral density of z fluctuations resulting from the nonconservative force is

$$|\tilde{z}_{\mathrm{nc}}(\omega)|^2 = \frac{16(k_{\mathrm{B}}T)^2 S_2^2}{\alpha_x \beta^3 \left(\omega^2 + \frac{4\alpha_x^2}{\beta^2}\right)\left(\omega^2 + \frac{\alpha_z^2}{\beta^2}\right)}, \tag{5}$$

where we set $\alpha_x = \alpha_y$ for clarity.

The Fourier spectra of the thermal and nonconservative forces are shown for the case of a large particle in Fig. 2(a) and for a small particle in Fig. 3(a) (using both the full scattering form and its second-order expansion). The Fourier spectra of the fluctuations in z driven by the thermal and nonconservative forces are shown in Figs. 2(b) and 3(b). Precise agreement is found between the analytical spectra, indicated by solid curves, and the simulations. It is clear from these spectra that the characteristic time scale of nonconservative fluctuations is determined by the x-y dynamics of the particle, rather than by the circulation time inferred from data in Figs. 1(c) and 1(d). The uncertainty in a measurement of the particle position is found by integrating the spectral density over the bandwidth of the measurement. However, the total root mean square (RMS) fluctuations of the thermal and nonconservative components of the displacement, z_{T} and z_{nc} (integrated over all frequencies) are a useful practical measure of noise in experiments where the localization of the particle is of primary importance. We find that the standard deviation for thermal fluctuations is $\sigma_{\mathrm{T}} = (\frac{k_B T}{\alpha_z})^{1/2}$, and for nonconservative fluctuations is $\sigma_{\mathrm{nc}} = \frac{10\, S_2 k_B T}{\sqrt{11}\alpha_x^2}$ (where we set $\alpha_x = \alpha_y = 5\alpha_z$). These are plotted as a function of x stiffness in the insets of Figs. 2(b) and 3(b), with the assumption that the scattering force and trap stiffness

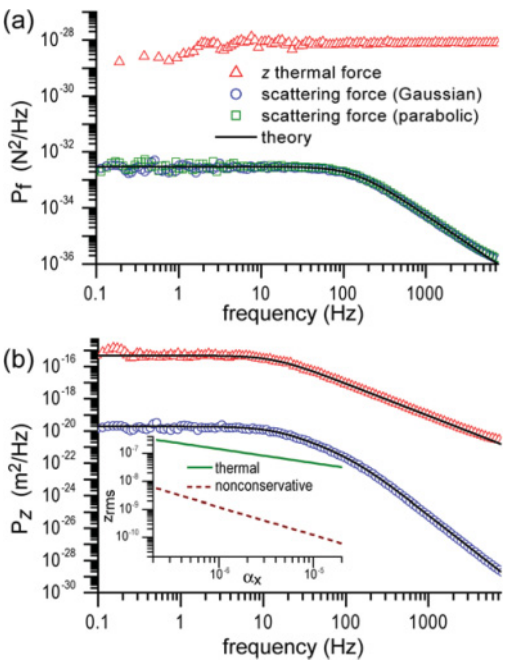

FIG. 3. (Color online). Similar to Fig. 2, except the particle is assumed to be small compared with the wavelength, and the scattering profile is assumed to have a Gaussian form which corresponds to the intensity profile of the trapping beam at the trap center. Physical parameters are identical to those used in the small-particle simulation in Fig. 1.

both scale linearly with the trap optical power P. The ratio of the standard deviations of nonconservative and thermal fluctuations scales as $P^{-1/2}$, indicating that the importance of the nonconservative effect decreases as the trap becomes stiffer. Using the physical parameters chosen for the spectra in Fig. 2, the RMS fluctuations arising from the direct thermal fluctuations are ~1000 times larger than those arising from the scattering force. Since the thermal and nonconservative noise sources are uncorrelated and add in quadrature, the augmentation of the amplitude of total fluctuations is <1 part in 10^6.

IV. APPLICATION TO A REALISTIC FORCE FIELD

In the preceding section, we have shown that the simplified system, consisting of a harmonic trapping force and an axial scattering force which depends only on ρ, reproduces the nonequilibrium probability flux which is the main feature of the nonconservative scattering force. The simplifications facilitated an analytical calculation of the level of excess noise introduced by the nonconservative force. In this section we consider a realistic system, in which the gradient (trapping) and scattering forces are derived from the three-dimensional Gaussian optical mode. Although this realistic system contains nonlinearities, cross talk between axial and transverse dynamics, and a scattering force which is no longer purely axial, we will show that the analytic calculations derived from the simplified model accurately predict scattering force fluctuations observed in simulations of the realistic system.

In the realistic simulation we take the gradient force to be proportional to the gradient of the optical intensity and the scattering force to be proportional to the local Poynting vector, which is proportional to the intensity itself and acts along the phase gradient direction [13]. This form is appropriate for a small particle, but can also be used as a highly accurate parametrization of the measured force on a finite-size particle as a function of displacement in experiments. The three-dimensional, nonlinear force functions introduce new effects not present in the linearized system. Differential stiffness decreases with distance from the geometrical center of the trap. In addition, the optical mode spreads as it propagates past the trap center, and as a result there is a decrease in the transverse restoring force with increasing z in the neighborhood of the effective trap center. The spreading of the optical mode also causes the scattering force to weaken with increasing z as well as with increasing ρ. The z dependence of the intensity gradient and scattering forces will cause transverse force fluctuations to arise from axial position fluctuations, which was not included in the simpler model previously introduced. The question arises whether these additional effects result in an increase in fluctuations of the particle position.

To address this issue we run the simulation of a particle subject to the scattering force vector and gradient force based on the three-dimensional Gaussian mode [13]. However, in this case the scattering force includes a conservative contribution which can be represented as the gradient of a potential, as we explain later. In the neighborhood of the effective trap center the z component of the scattering force decreases with increasing z. This predominantly linear dependence of the axial scattering force on z serves as an enhancement of the axial restoring force experienced by the particle—the particle is more strongly trapped in the presence of the z-dependent scattering force than it would be if the scattering force were independent of z. The z dependence of the axial scattering force can therefore be represented by a potential, and does not contribute to the nonequilibrium effects that result from nonconservative forces. We therefore decompose the scattering force into conservative and nonconservative components and calculate the power spectra of the two components separately. The decomposition is done as follows. The magnitude of the full scattering force is of the form

$$\vec{F}_s(x,y,z) = F_0\left(\frac{1}{1+z^2/z_0^2}\right)\exp\left[\frac{-2(x^2+y^2)}{\omega_0^2\left(1+z^2/z_0^2\right)}\right]\hat{S},$$

where $\hat{S}$ is a unit vector in the direction of the Poynting vector (which corresponds to the phase gradient direction), ω_0 is the Gaussian spot size, and z_0 is the Rayleigh distance, $z_0 = \frac{\pi\omega_0^2 n}{\lambda}$. We wish to calculate the potential whose gradient most closely matches the total scattering force in the region visited by the particle. The difference between the actual scattering force and this conservative approximation would represent the nonconservative component of the scattering force. Since the particle is confined to a small volume centered on the beam axis, it is sufficient to choose the conservative component of the scattering force to duplicate the z dependence of the z component of the scattering force on the beam axis, $\vec{F}_{\rm sc}(z) = \vec{F}_s(0,0,z)$, where the lack of x and y dependence is determined by the criteria that $\vec{F}_{\rm sc}(z)$ is conservative. The nonconservative component is obtained by subtracting the conservative component from the full scattering force, $\vec{F}_{\rm snc}(x,y,z) = \vec{F}_s(x,y,z) - \vec{F}_{\rm sc}(z)$. Making use of this decomposition of the scattering force, the effective conservative force acting on the particle is the combination of the intensity gradient force and the conservative component of the scattering force. The remainder of the scattering force, $\vec{F}_{\rm snc}(x,y,z)$, contains the transverse dependence of the scattering force and is the driving term for nonconservative effects.

Figure 4 shows the fluctuations in the scattering force in a simulation using the three-dimensional restoring and scattering forces. The decomposition into conservative and nonconservative components only applies to the calculation of the power spectra of the scattering force; the particle dynamics are generated from the full scattering force. The system parameters are comparable to those used to produce Fig. 3, although the effective trap power has been increased by a factor of ~5% to maintain the same effective trap stiffness at the equilibrium point in the nonlinear simulation. The scattering profile, adopting the small-particle limit, is strictly defined by the three-dimensional optical mode, resulting in a Gaussian profile with standard deviation $\sigma = \omega(z)/2$ where $\omega(z)^2 = \omega_0(1+z^2/z_0^2)$. The value of ω_0 has been set to 0.411 μm in order to obtain the nominal 5:1 ratio between axial and transverse stiffness that we use to evaluate our analytical theory. The resulting scattering profile is narrower than the one that was used in the previous simulations and results in somewhat stronger scattering fluctuations in Fig. 4.

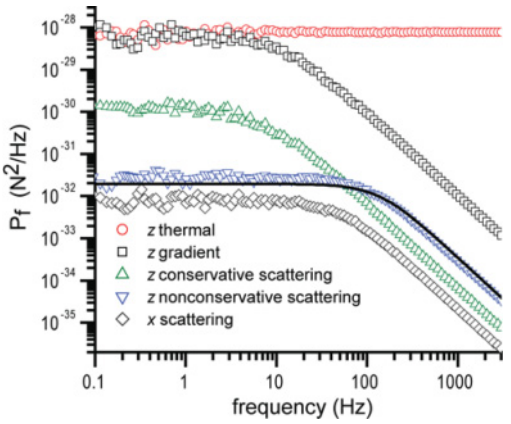

FIG. 4. (Color online). Power spectra of force components acting on a small particle assuming the gradient force and scattering force are proportional to the intensity gradient and Poynting vector, respectively, of the three-dimensional Gaussian optical mode. Fourier spectral density of the thermal driving force (circles), axial gradient force (squares), conservative axial component of the scattering force (triangles), nonconservative axial component of the scattering force (inverted triangles), and the x component of the scattering force (diamonds). The solid line represents the analytical calculation of the nonconservative scattering force contribution predicted by Eq. (4). The time step is 5 μs, and the physical parameters are $\alpha_x = \alpha_y =$ 2.01 pN/μm, and $\alpha_z = 0.360$ pN/μm and $F_0 = 0.04$ pN (evaluated at the effective trap center) using the point particle approximation with $\omega_0 = 0.411$ μm. The effective z stiffness contains a contribution of 0.026 pN/μm from the conservative component of the scattering force.

Figure 4 has several interesting features. The thermal force spectrum $|\tilde{F}_T(\omega)|^2$ and the intensity gradient force spectrum $|\tilde{F}_g(\omega)|^2$ correspond closely at low frequency. Comparison of the phases of the two spectra (not shown) indicates they are anticoherent. This is consistent with the fact that low-frequency wandering of the particle is largely suppressed by the optical trap, which implies that the gradient force neutralizes the thermal force at low frequency. Above the characteristic frequency $f_0 = \alpha_z/2\pi\beta$ of axial fluctuations, the spectrum of the gradient force falls below that of the thermal forcing, consistent with the fact that high-frequency jiggling of the particle is relatively unaffected by the trapping potential. The spectrum of the conservative component of the scattering force $|\tilde{F}_{sc}(\omega)|^2$ is similar to that of the gradient force, but at lower amplitude. These spectra are phase coherent and confirm a slight enhancement of the restoring force by the conservative component of the scattering force. The spectrum of the z component of the nonconservative scattering force component $|\tilde{F}_{snc}(\omega)|^2$ represents the driving force for nonconservative fluctuations. Unlike $|\tilde{F}_{sc}(\omega)|^2$, it is generated by x-y motion of the particle and its dependence on the z coordinate has been subtracted off. It therefore acts as a generator of independent axial fluctuations, rather than as a component of the restoring force. The solid line shows the prediction of Eq. (4) for $|\tilde{F}_{snc}(\omega)|^2$, using the effective stiffness (including contributions from the gradient and conservative scattering forces) and the on-axis scattering force F_0, both evaluated at the effective trap center. There is good agreement between the analytical calculation based on the linearized system and the dynamics found in the fully nonlinear system. The level of fluctuations in the simulation is slightly in excess of the analytical prediction, apparently because the trap is barely stable for these parameters and the particle transiently wanders from the effective trap center to regions where the effective stiffness is smaller than the nominal value. This small discrepancy vanishes if the trap power is increased by a factor of 2 or more. The spectrum of force fluctuations associated with the nonconservative component of the scattering force is nearly four orders of magnitude below the direct thermal forcing. Figure 4 also shows the spectrum of fluctuations in the x (tangential) component of the scattering force, which is smaller than both the conservative and nonconservative components of the axial scattering force, and is therefore not a significant source of additional fluctuations.

The decomposition of *position* fluctuations into components arising from distinct forcing terms that was performed in the linear system is no longer possible in the nonlinear system. However, the relative strengths of forcing from conservative and nonconservative forces have been calculated with high precision, and there is no reason to believe that the nonlinear effects or cross terms in the realistic model would preferentially amplify force fluctuations originating from nonconservative relative to those originating from thermal fluctuations. Therefore the increase in position fluctuations in the presence of nonconservative effects should be in proportion to the increase in force fluctuations. No significant excess fluctuations were detected in the spectra of x, x^2, and z when comparing the simulation of the nonlinear system to one based on an equivalent linear system (data not shown), confirming that the additional dynamic processes present in the nonlinear model (nonlinearities and cross terms in the equations of motion) do not change the character or amount of fluctuations introduced by the nonconservative force term.

V. ADDITIONAL FLUCTUATIONS WHEN STRETCHING A DNA TETHER

The previous results apply to the case where there is no external force on the trapped particle and it remains in the neighborhood of the effective trap center. In single-molecule biophysics experiments, the optical trap is typically used to apply a substantial force to a biological macromolecule, and the equilibrium position, taking into account the external force, will no longer lie on the beam axis. In this regime the scattering force will no longer be an even function of the displacement x or y from the equilibrium position and may have a substantial nonaxial component. As in the previous section, where the nonlinearity of the system prevents us from decomposing the motion into components arising from distinct forcing terms, we can gain insight into the level of nonequilibrium fluctuations by measuring fluctuations of the scattering force itself in a realistic simulation.

We model an experiment in which the optical trap is used to measure variations in the length of a DNA tether. We assume the DNA is anchored to a cover slip, the tether making a 45° angle with the beam axis. As in Fig. 4, we assume that the scattering force and gradient force are proportional to the local Poynting vector and intensity gradient vector, respectively, of

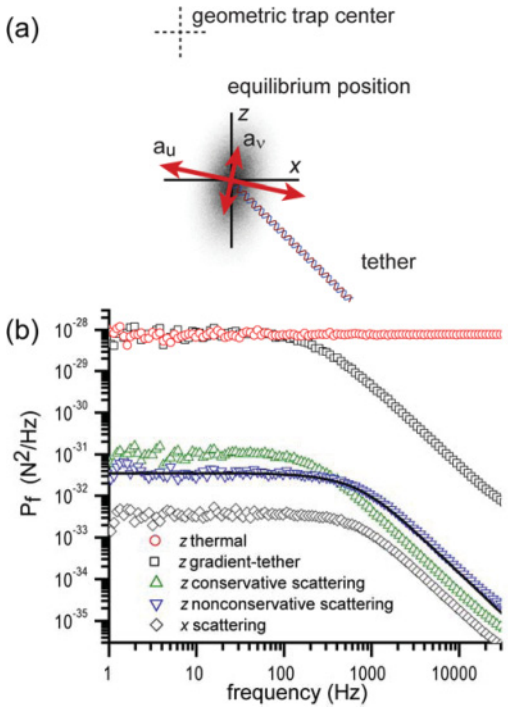

FIG. 5. (Color online). Simulation of a particle tethered by a DNA molecule at 45°, in which the tether attachment point is displaced from the trap center in the x-z plane such that the tension in the DNA is three-fourths of the maximum force the trap can exert at 45°. (a) Schematic illustrates the effective conservative force characteristics for the particle. The combined gradient force, conservative component of the scattering force, and tether force were linearized around the equilibrium point. The principal axes of the resulting elasticity tensor are illustrated by arrows which are superimposed on the probability density function of particle position obtained in the simulation. (b) Fourier spectral density of the thermal driving force (circles), combined gradient and tether force (squares), conservative axial component of the scattering force (triangles), nonconservative axial component of the scattering force (inverted triangles), and the x component of the scattering force (diamonds). The solid curve represents the analytical calculation of the nonconservative scattering force contribution, as described in the text. Simulations performed at tension 1.2 pN with $r_p = 0.250\ \mu$m, Gaussian spot size $\omega = 0.411\ \mu$m, and $F_0 = 0.4$ pN. The effective stiffnesses are $a_u = 21.7$ pN/μm and $a_v = 6.4$ pN/μm with $\phi = -10°$.

the three-dimensional Gaussian mode of the trapping beam [13]. The attachment point is chosen so that the force exerted on the tether is three-fourths of the maximum force that the optical trap can produce at 45°, well past the regime of a linear restoring force. Unlike the simulation illustrated in Fig. 4, the particle is sufficiently far from the trap center that cross terms, such as the dependence of nonaxial force on axial position, and vice versa, are substantial. The force vs extension curve of the DNA tether is calculated using the Marko-Siggia wormlike chain model with contour length of 2.0 μm [14].

Force fluctuations in the simulation of a tether experiment are shown in Fig. 5. The curves shown in Fig. 5(b) correspond to those shown in Fig. 4, except that the effective potential experienced by the particle includes the tension in the DNA tether. As in Fig. 4, the spectrum of the combined restoring force (including the gradient force and the tether force) cancels the thermal force at low frequency. The conservative part of the scattering force opposes the gradient force (since the particle is pulled to negative z by the DNA tether) but is small compared to the gradient and tether forces. The spectra of the nonconservative components of the scattering force (axial and nonaxial) are again far below the level of the thermal force spectrum.

The theoretical framework previously defined can be used to calculate the nonconservative nonaxial scattering force fluctuations. In the present case, assuming the attachment pulls the particle away from the beam axis along the x direction, the expansion of the axial scattering force about equilibrium position will have a nonzero first-order term, $\vec{F}_s = (S_0 + S_1 x)\hat{z}$. To first order in the displacement x, the spectrum of scattering force fluctuations can be obtained by simply multiplying the spectrum of x fluctuations by S_1. However, the spectrum of x fluctuations is more complex for a trapped particle which is tethered to the surface than for an otherwise unconstrained particle. For a free particle trapped on the beam axis the motion is easily resolved into axial and transverse components, which have different effective stiffnesses. The tethered particle experiences a more complex force field which is the combination of the optical trap and DNA elasticity. By combining the effective potential energy arising from the optical trap, the tether elasticity, and the conservative portion of the scattering force, we can define the total potential energy of the particle as a function of position, $U(x,y,z)$. To first order the force arising from a small displacement in an arbitrary direction is found by multiplying the displacement vector by the Hessian matrix of $U(x,y,z)$. However, the Hessian evaluated at the equilibrium position is not diagonal, meaning a displacement along the x, y, or z coordinate axis results in a force which is generally not parallel to the displacement. The eigenvectors of the Hessian matrix, however, define a coordinate system in which the Hessian matrix is diagonal, and in which its diagonal elements are the stiffnesses for displacement along the corresponding eigenvectors. The dynamics along the three eigenvectors are independent and governed by the corresponding stiffness. (This procedure is not necessary for the particle trapped on the beam axis because the axial and transverse directions themselves are eigenvectors.) The result of this analysis is illustrated in Fig. 5(a). Two eigenvectors lying in the x-z plane are superimposed on a probability density function of the particle position in the simulation. The axis of maximum stiffness, labeled u, makes an angle $\phi = -10°$ with the positive x axis while the stiffness along the eigenvector v is a factor of 3 smaller (see Fig. 5 caption for values). As expected, the maximum observed particle fluctuations are along the axis of smallest stiffness.

The spectrum of nonconservative axial force fluctuations is predicted as follows. The power spectrum of position fluctuations along each of the principal axes is calculated from Eq. (3), using the corresponding values of α. The projections of these fluctuations on the x direction are calculated, and since the dynamics corresponding to different principal axes are independent, the projected power spectra are additive. The resulting combined spectrum is multiplied by S_1 to obtain the spectrum of nonconservative axial force fluctuations. The solid line shows this calculated spectrum,

which agrees precisely with the measured fluctuation spectrum of the nonconservative component of the axial scattering force.

The same considerations applying to Fig. 4 apply here. Due to the nonlinear nature of the equation of motion fluctuations of particle position cannot be decomposed into components arising from conservative and nonconservative forcing terms. However, the additional force fluctuations introduced by the ρ dependence of the axial and nonaxial components of the scattering are very small compared with the other fluctuating forces. Since there is no reason to assume that nonconservative fluctuations will be amplified disproportionately compared to fluctuations arising from conservative forces, the nonconservative forces are not expected to cause an appreciable degradation in a measurement of the tether length.

Our general conclusion is that the method of calculating additional fluctuations associated with the nonconservative scattering force that we developed in the context of the simplified model can be applied to this experimental configuration, provided the system is linearized about the equilibrium point and that transverse dependence of the scattering force is represented by a Taylor expansion. As in the case of the simplified model, the additional fluctuations associated with the nonconservative force are small. The main effect of the scattering force is a slight reduction in the effective stiffness of the optical trap in the neighborhood of the equilibrium point.

VI. CONCLUSION

In conclusion, we have introduced a simplified model of trapping with a nonconservative scattering force which fully reproduces the nonequilibrium flux reported previously, and which allows us to identify a distinct noise mechanism associated with the nonequilibrium flux. The model correctly predicts fluctuations in simulations of the simplified system, of the fully nonlinear system and of a system including a DNA tether, provided that the transverse dependence of the scattering force is represented as a Taylor series in ρ and the effective potential experienced by the particle is linearized about the effective equilibrium point. The additional fluctuations are extremely broadband, in contrast to the extremely long time period that characterizes the net circulation rate. Although the effect is small for typical configurations, the formulas obtained establish the dependence of this additional noise on the system parameters and can be used to guide the design of an experiment that would maximize or minimize the effect. A realistic simulation of an experiment in which the length of a DNA molecule is measured indicates that the additional RMS fluctuations associated with the scattering force in a typical experimental configuration do not significantly increase the experimental uncertainty in this common type of measurement. The most significant effect of the scattering force in such experiments is modification of the effective stiffness of the trap.

[1] A. Ashkin, Phys. Rev. Lett. **24**, 156 (1970).
[2] W. Denk and W. W. Webb, Appl. Opt. **29**, 2382 (1990).
[3] A. Pralle, M. Prummer, E.-L. Florin, E. H. K. Stelzer, and J. K. H. Horber, Microsc. Res. Tech. **44**, 378 (1999).
[4] A. Rohrbach, E. H. K. Stelzer, J. Appl. Phys. **91**, 5474 (2002).
[5] E. A. Abbondanzieri, W. J. Greenleaf, J. W. Shaevitz, R. Landick, and S. M. Block, Nature (London) **438**, 460 (2005).
[6] A. Ashkin, Biophys. J. **61**, 569 (1992).
[7] Y. Roichman, B. Sun, A. Stolarski, and D. G. Grier, Phys. Rev. Lett. **101**, 128301 (2008).
[8] B. Sun, J. Lin, E. Darby, A. Y. Grosberg, and D. G. Grier, Phys. Rev. E **80**, 010401(R) (2009).
[9] P. Wu, R. Huang, C. Tischer, A. Jonas, and E.-L. Florin, Phys. Rev. Lett. **103**, 108101 (2009).
[10] G. Pesce, G. Volpe, A. C. de Luca, G. Rusciano, and G. Volpe, Europhys. Lett. **86**, 38002 (2009).
[11] B. Sun and D. G. Grier, e-print arXiv:0807.1242v1 (2008).
[12] See Supplemental Material at http://link.aps.org/supplemental/10.1103/PhysRevE.84.031108 for the derivation of the Fourier spectrum of the nonconservative force and details on the characterization of the restoring force in the presence of a DNA tether.
[13] A. Yariv, *Optical Electronics*, 3rd ed. (John Wiley & Sons, New York, 1988).
[14] J. F. Marko and E. D. Siggia, Macromolecules **28**, 8759 (1995).